**IEEE Sensors Council**

All-Parameter System-Level Calibration for SINS/CNS based on global observability analysis

Zhihao Xu, Zhaofa Zhou, Zhenjun Chang, Shiwen Hao and Hui Duan

Abstract—**Before using the strap-down inertial navigation system (SINS)/ celestial navigation system (CNS) integrated navigation system, the calibration of its error parameters is a necessary process to improve the system accuracy. In this paper, an all-parameter system-level calibration method has been proposed, which utilizes Kalman filtering for simultaneously estimating the bias, scale factor, misalignments of inertial measurement unit (IMU), and installation errors of the star sensor. The observation has been constructed using the inertial navigation output information and the starlight vector measured by the star sensor. The observability of the error parameters has been analyzed theoretically, and the optimal excitation conditions for each error parameter are obtained. The effects of the angle between the starlight vector and the optical axis of the star sensor, and the attitude of the IMU, on the estimation accuracy of the installation error of the star sensor are also given. Finally, a 10-order rotation scheme has been designed and all the error parameters can be optimally excited. The simulation and experimental results demonstrate that all the error parameters have better stability and repeatability, when compared with the traditional method, and the initial alignment error of 3.4" is better than 13.1" of the traditional method. Moreover, the installation error of the star sensor can be estimated with a high precision only when the angle between the starlight vector and the optical axis of the star sensor exceeds 1°. It is shown that the proposed method can effectively improve the navigation performance of the SINS/CNS integrated navigation system.**

Index Terms—**all-parameter system-level calibration, global observability analysis, Kalman filter, SINS/CNS integrated navigation system, 10-order rotation scheme**
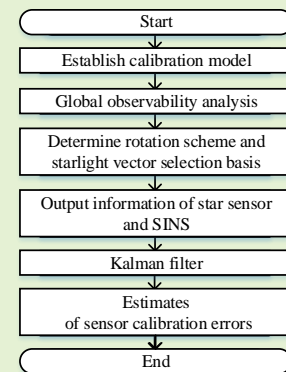
I. INTRODUCTION

THE Strap-Down Inertial Navigation System (SINS) has the advantages of strong autonomy, anti-interference, and continuous information output, despite the decrease of the navigation accuracy with the passage of time owing to the existence of sensor error [1]. The Celestial Navigation System (CNS) has the advantages of complete autonomy, high reliability, and high accuracy of long-time measurement, despite a discontinuous information measurement. Owing to their complementary advantages, SINS/CNS integrated navigation has become a typical integrated navigation mode [2], [3], which is extensively employed in ships, aircraft, missiles, and other military equipment [4].

Inertial Measurement Unit (IMU) is the core hardware of SINS, and even a very small IMU sensor error will entail a large navigation error in the navigation process [5], [6]. The measurement accuracy of the star sensor, which is the core equipment in CNS, can reach arc-seconds, though its installation error can reach arc-minutes [7]. This is one of the main factors that delimits the accuracy of the SINS/CNS integrated navigation [8]. These error parameters must be

calibrated before use to improve the navigation accuracy of the system. The traditional method is a separated calibration of the IMU error parameters and the installation error of the star sensor. Currently, the calibration methods of IMU mainly include the separated calibration and system-level calibration. The separated calibration method directly invokes the output of the gyroscope and the accelerometer as the observational quantity to identify the error parameters [9], [10]. Although this method is simple with respect to the modeling and calculation, its calibration accuracy is restricted owing to the turntable [11], [12]. The system-level calibration technology has become the primary research to calibrate the error parameters conveniently, comprehensively, and economically [13], [14].

The system-level calibration employs the velocity or position errors of the navigation output as an observation to identify the error parameters [15], [16]. The key is to fully consider the observability of the IMU error parameters, and reasonably arrange the rotation scheme, besides achieving a sufficient estimation of the error parameters [17]. To pre-assess the estimated effect of the error parameters, the observability analysis of the system should be carried out in advance to determine the rotation scheme [18]. An unreasonable rotation scheme may result in the inability to effectively estimate certain error parameters, and excessive rotations complicate the calibration process and extends the calibration time. The optimal rotation norm calibration method adopted by Wang *et al*. [19] can calibrate 21 error parameters. Although only six positions are required, it needs up to 40 rotations. Li *et al*. [20]

have proposed an analytical/extended Kalman filter integrated calibration method, which designs four rotations and eleven positions for analytical calibration and fine calibration. Gao *et al.* [21] have adopted a least-squares fitting self-calibration method, which can calibrate 23 error parameters. It needs to be calibrated in three steps, thus entailing a complicated rotation process and an extended calibration time. Hu *et al.* [16] have employed a novel method to calibrate the installation error of the inertial navigation system based on the attitude error model and attitude difference, which has the issue of poor accuracy for certain parameters. Camperlein and Mazzanti [22] have proposed an 18-order calibration scheme. An improved 18-order calibration method has been proposed by Cai *et al.* [23]. Yuan *et al.* [24] have designed a 15-order rotation scheme. These methods have been proved by experiments that they can effectively calibrate the error parameters. However, they lack the theoretical analysis of the rotation scheme, and the calibration time is long.

Several scholars have studied the calibration method of the installation error between the star sensor and the SINS. A traditional approach is to perform a two-bit flip calibration with a single star simulator on marble, and taking the output of the accelerometer and the star simulator information as a reference [25]. An alternative approach is to calibrate with a navigation solver to capture the installation error. Gao *et al.* [26] have utilized the attitude information output by inertial navigation and star sensor to calibrate the installation error. However, it is difficult for the narrow field of view (NFOV) star sensor to obtain the attitude information through a single observation. Wang *et al.* [27] have adopted the difference between the quaternion and the angular velocity between the star sensor and the gyroscope as a measurement to calibrate the installation error. The premise of these methods is that the IMU must have been calibrated, and the calibration residual is inevitably induced into the calibration of the installation error of the star sensor, besides ignoring the influence of the multiple start-ups of the IMU on the error of the inertial device. Yang *et al.* [28] have taken the angle between the starlight vector and the gravity vector as the measurement to estimate the gyro error parameters and the installation error of the star sensor.

This work proposes a system-level calibration method for SINS/CNS integrated navigation system. Compared with the traditional calibration method, it has the following advantages.

1) The error parameters of the IMU and the star sensor can be calibrated simultaneously, thus reducing the calibration process and the influence of multiple startups of the IMU. The method is more conducive for the estimation of gyro error parameters, and it avoids a direct inducing the estimated residuals of the IMU error parameters into the installation error of the star sensor.

2) The optimal excitation conditions of each error parameter have been obtained, and the difference of the optimal observability of each parameter is determined. The theoretical basis is provided for the 10-order rotation scheme, hence the calibration of the error parameters can be completed in a shorter period with less rotation times.

3) The coupling relationship between the attitude error and the installation error of the star sensor has been analyzed in detail. The effects of the angle between the starlight vector and the optical axis of the star sensor and the attitude of the IMU, on the estimation accuracy of the installation error of the star sensor are given. The basis of star selection has been determined, and the estimation accuracy of the installation error of the star sensor is improved.

The paper is organized as follows: In Section 2, the error model and Kalman filter have been established. Section 3 presents a detailed observability analysis of the system and designs a 10-order rotation scheme. In Section 4, the performance of the algorithm is verified by simulations and experiments. Finally, the conclusions are given in Section 5.

II. PRINCIPLE OF CALIBRATION METHOD

The error parameters are calibrated using a Kalman filter. The difference between the starlight vector measured by the star sensor and the starlight vector obtained by the inertial navigation solution, has been used in the measurement, and the zero velocity is also included in the observation data. The all-parameter estimation is realized by multiple rotations, and the principle is illustrated in Fig. 1.
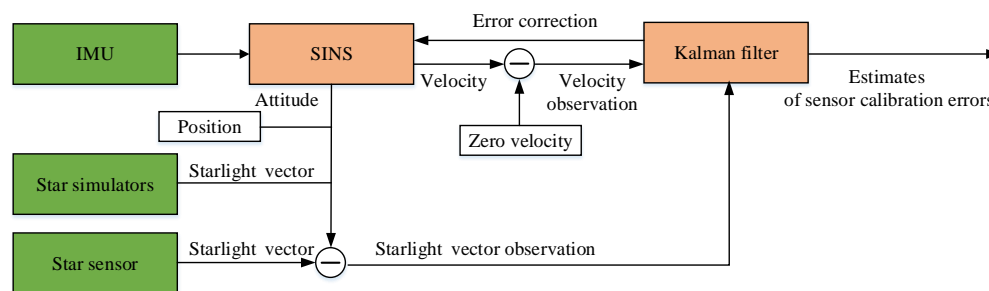
Fig. 1. Principle of the system-level calibration method for SINS/CNS.

A. Coordinate Frame Introduction

A number of coordinate frames have been defined and described as follows.

The earth frame (*e*-frame) takes the center of the earth as the origin, where the *x*-axis is located in the equatorial plane and the points to the zero-degree longitude. Further, the *z*-axis points to the direction of the earth axis.

The navigation frame (*n*-frame), select the east-north-up (ENU) frame as the navigation frame.

The body frame (*b*-frame) is rigidly attached to the body carrying the navigation system and defined as right-forward-upward.

The mathematical platform frame (*p*-frame) is the navigation frame determined by the attitude of the SINS solution.

The star sensor frame (*s*-frame) takes the center of the image plane as the origin, with the *z*-axis perpendicular to the focal plane and the *x*-axis and *y*-axis satisfying the right-hand rule.

B. IMU Error Model

The gyros and accelerometers that form the basis of SINS play a critical role in the navigation performance. Before the system can be put into service, it needs to be calibrated to remove the major aberrations that can induce errors in the navigation system calculations. The error model of the gyro is presented as

$$\begin{bmatrix} \delta\omega_x \\ \delta\omega_y \\ \delta\omega_z \end{bmatrix} = \begin{bmatrix} \delta K_{gx} & \delta K_{gxy} & \delta K_{gxz} \\ \delta K_{gyx} & \delta K_{gy} & \delta K_{gyz} \\ \delta K_{gzx} & \delta K_{gzy} & \delta K_{gz} \end{bmatrix} \begin{bmatrix} \omega_x \\ \omega_y \\ \omega_z \end{bmatrix} + \begin{bmatrix} \varepsilon_x \\ \varepsilon_y \\ \varepsilon_z \end{bmatrix} + \begin{bmatrix} \varpi_{gx} \\ \varpi_{gy} \\ \varpi_{gz} \end{bmatrix} \quad (1)$$

where $\delta\omega_i$ is the output error of the angular rate along i-axis and ω_i is the actual value. $\delta K_{gi}, \delta K_{gij}$, and ε_i ($i=x, y, z, j=x, y, z, i \neq j$) represent the gyro scale factor, installation error and constant drift, respectively, in the b-frame. Here ϖ_{gi} is the angular random walk noise in i-axis.

The error model of the accelerometer is presented as

$$\begin{bmatrix} \delta f_x \\ \delta f_y \\ \delta f_z \end{bmatrix} = \begin{bmatrix} \delta K_{ax} & 0 & 0 \\ \delta K_{ayx} & \delta K_{ay} & 0 \\ \delta K_{azx} & \delta K_{azy} & \delta K_{az} \end{bmatrix} \begin{bmatrix} f_x \\ f_y \\ f_z \end{bmatrix} + \begin{bmatrix} \nabla_x \\ \nabla_y \\ \nabla_z \end{bmatrix} + \begin{bmatrix} \varpi_{ax} \\ \varpi_{ay} \\ \varpi_{az} \end{bmatrix} \quad (2)$$

where δf_i is the output error of the specific force in i-axis and f_i is the actual value. $\delta K_{ai}, \delta K_{aij}$, and ∇_i ($i=x, y, z, j=x, y, z, i \neq j$) represent the accelerometer scale factor, installation error, and constant bias, respectively, in the b-frame. ϖ_{ai} is the velocity random walk noise in i-axis.

C. Star Sensor Installation Error Model

Generally, the installation of the star sensor cannot guarantee the coincidence of the s-frame and the b-frame, hence the installation matrix between the s-frame and the b-frame is not a unit matrix. Suppose $\boldsymbol{r}^b$ and $\boldsymbol{r}^s$ represent the coordinates of the same vector in the s-frame and the b-frame, respectively, then there is the following relationship

$$\boldsymbol{r}^b = \boldsymbol{C}_s^b \boldsymbol{r}^s \quad (3)$$

where,

$$\boldsymbol{C}_s^b = \begin{bmatrix} \cos\mu_z\cos\mu_y - \sin\mu_z\sin\mu_x\sin\mu_y & -\sin\mu_z\cos\mu_x & \cos\mu_z\sin\mu_y + \sin\mu_z\sin\mu_x\cos\mu_y \\ \sin\mu_z\cos\mu_y + \cos\mu_z\sin\mu_x\sin\mu_y & \cos\mu_z\cos\mu_x & \sin\mu_z\sin\mu_y - \cos\mu_z\sin\mu_x\cos\mu_y \\ -\cos\mu_x\sin\mu_y & \sin\mu_x & \cos\mu_x\cos\mu_y \end{bmatrix}$$

$\boldsymbol{\mu} = \begin{bmatrix} \mu_x & \mu_y & \mu_z \end{bmatrix}^T$ is the installation error angle of the star sensor.

In practice, the mechanical mounting can generally reduce the mounting error to a small angle. Neglecting the higher-order terms, $\boldsymbol{C}_s^b$ can be written as

$$\boldsymbol{C}_s^b \approx \begin{bmatrix} 1 & \mu_z & -\mu_y \\ -\mu_z & 1 & \mu_x \\ \mu_y & -\mu_x & 1 \end{bmatrix} = \begin{bmatrix} \boldsymbol{I} - (\boldsymbol{\mu}\times) \end{bmatrix} \quad (4)$$

D. Design of Kalman Filter

According to the strap-down inertial navigation error model, taking the position error as a measurement is only conducive for the observability of the velocity error. Therefore, when the velocity error has been used as the measurement, the position error is not used as the state variable to reduce the system dimension. A 30-dimensional Kalman filter is established for the system-level calibration, and the system state vector is

$$\boldsymbol{X} = \begin{bmatrix} \boldsymbol{\phi}^n & \delta\boldsymbol{V}^n & \delta\boldsymbol{K}_g & \delta\boldsymbol{K}_{gg} & \boldsymbol{\varepsilon}^b & \delta\boldsymbol{K}_a & \delta\boldsymbol{K}_{aa} & \boldsymbol{\nabla}^b & \boldsymbol{\mu} \end{bmatrix}^T \quad (5)$$

where $\boldsymbol{\phi}^n = [\phi_E \quad \phi_N \quad \phi_U]^T$ is the misalignment angle in the n-frame, $\delta\boldsymbol{V}^n = [\delta V_E \quad \delta V_N \quad \delta V_U]^T$ is the velocity error, $\delta\boldsymbol{K}_g = [\delta K_{gx} \quad \delta K_{gy} \quad \delta K_{gz}]^T$ is the gyro scale coefficient error, $\boldsymbol{K}_{gg} = [\delta K_{gxy} \quad \delta K_{gxz} \quad \delta K_{gyx} \quad \delta K_{gyz} \quad \delta K_{gzx} \quad \delta K_{gzy}]^T$ is the gyro installation error, $\boldsymbol{\varepsilon}^b = [\varepsilon_x \quad \varepsilon_y \quad \varepsilon_z]^T$ is the gyro constant drift, $\delta\boldsymbol{K}_a = [\delta K_{ax} \quad \delta K_{ay} \quad \delta K_{az}]^T$ is the accelerometer scale coefficient error, $\delta\boldsymbol{K}_{aa} = [\delta K_{ayx} \quad \delta K_{azx} \quad \delta K_{azy}]^T$ is the accelerometer installation error, and $\boldsymbol{\nabla}^b = [\nabla_x \quad \nabla_y \quad \nabla_z]^T$ is the accelerometer constant bias.

The attitude and velocity error equations of the strap-down inertial navigation are given as

$$\begin{cases} \dot{\boldsymbol{\phi}} = \boldsymbol{\phi}\times\boldsymbol{\omega}_{in}^n + \delta\boldsymbol{\omega}_{in}^n - \boldsymbol{C}_b^n(\delta\boldsymbol{K}_g + \delta\boldsymbol{K}_{gg})\boldsymbol{\omega}_{ib}^b - \boldsymbol{C}_b^n\boldsymbol{\varepsilon}^b \\ \delta\dot{\boldsymbol{V}}^n = -\boldsymbol{\phi}^n\times\boldsymbol{f}^n + \boldsymbol{C}_b^n(\delta\boldsymbol{K}_a + \delta\boldsymbol{K}_{aa})\boldsymbol{f}^b \\ \quad + \delta\boldsymbol{V}^n\times(2\boldsymbol{\omega}_{ie}^n + \boldsymbol{\omega}_{en}^n) + \boldsymbol{V}^n\times(2\delta\boldsymbol{\omega}_{ie}^n + \delta\boldsymbol{\omega}_{en}^n) + \boldsymbol{\nabla}^b \end{cases} \quad (6)$$

Expand the above equation and write it as the system state equation

$$\dot{\boldsymbol{X}} = \boldsymbol{FX} + \boldsymbol{W}(t) \quad (7)$$

where $\boldsymbol{W}(t)$ is the output noise of the gyro and accelerometer. It is regarded as white noise.

$\boldsymbol{r}^e$ and $\boldsymbol{r}^s$ denote the unit vectors of the starlight vector generated by the star simulator in the e-frame and the s-frame, respectively. In the case of zero error, the unit vector $\boldsymbol{r}^e$ in the s-frame can be expressed as

$$\boldsymbol{r}^s = \begin{bmatrix} x_s \\ y_s \\ z_s \end{bmatrix} = \boldsymbol{C}_b^s \boldsymbol{C}_n^b \boldsymbol{C}_e^n \boldsymbol{r}^e = \begin{bmatrix} \boldsymbol{I}_{3\times 3} + (\boldsymbol{\mu}\times) \end{bmatrix} \boldsymbol{C}_n^b \boldsymbol{C}_e^n \boldsymbol{r}^e \quad (8)$$

where $\boldsymbol{C}_e^n = \begin{bmatrix} -\sin\lambda & \cos\lambda & 0 \\ -\sin L\cos\lambda & -\sin L\sin\lambda & \cos L \\ \cos L\cos\lambda & \cos L\sin\lambda & \sin L \end{bmatrix}$, λ is the local longitude and L is the local latitude.

Since the navigation information calculated by the inertial navigation contains errors, the vector $\hat{\boldsymbol{r}}^s$ obtained from the information output by the SINS is

$$\hat{\boldsymbol{r}}^s = \begin{bmatrix} \hat{x}_s \\ \hat{y}_s \\ \hat{z}_s \end{bmatrix} = \boldsymbol{C}_b^{s'}\boldsymbol{C}_p^b\boldsymbol{C}_e^n\boldsymbol{r}^e = \boldsymbol{C}_n^b\begin{bmatrix} \boldsymbol{I}_{3\times 3} + (\boldsymbol{\phi}\times) \end{bmatrix}\boldsymbol{C}_e^n\boldsymbol{r}^e \quad (9)$$

where $\boldsymbol{C}_p^b = \boldsymbol{C}_n^b\boldsymbol{C}_p^n = \boldsymbol{C}_n^b\begin{bmatrix} \boldsymbol{I} + (\boldsymbol{\phi}\times) \end{bmatrix}$, $\boldsymbol{C}_m^{s'}$ is the ideal star sensor installation matrix, which is the unit matrix.

Let $\Delta \boldsymbol{r}^s = \boldsymbol{r}^s - \hat{\boldsymbol{r}}^s$, then by taking (7) and (8) into it and discarding the high-order small quantities, we get

$$\Delta \boldsymbol{r}^s = (\boldsymbol{\mu} \times) \boldsymbol{C}_n^b \boldsymbol{C}_e^n \boldsymbol{r}^e - \boldsymbol{C}_n^b (\boldsymbol{\phi} \times) \boldsymbol{C}_e^n \boldsymbol{r}^e = \boldsymbol{M}_1 \boldsymbol{\mu} + \boldsymbol{M}_2 \boldsymbol{\phi} \quad (10)$$

where $\boldsymbol{M}_1 = -\left(\boldsymbol{C}_n^b \boldsymbol{C}_e^n \boldsymbol{r}^e\right) \times$, $\boldsymbol{M}_2 = \boldsymbol{C}_n^b \left[\left(\boldsymbol{C}_e^n \boldsymbol{r}^e\right) \times\right]$.

The difference between the vector measured by the star sensor and the vector calculated by the inertial navigation is utilized as the measurement. It includes the carrier attitude and star sensor installation errors, and then the filter quantity measurement $\boldsymbol{Z}_1$ is given as

$$\boldsymbol{Z}_1 = \Delta \boldsymbol{r}^s = \begin{bmatrix} \Delta x_s \\ \Delta y_s \\ \Delta z_s \end{bmatrix} = \begin{bmatrix} x_s \\ y_s \\ z_s \end{bmatrix} - \begin{bmatrix} \hat{x}_s \\ \hat{y}_s \\ \hat{z}_s \end{bmatrix} \quad (11)$$

The system measurement equation can be written as

$$\boldsymbol{Z}_1 = \boldsymbol{H}_1 \boldsymbol{X} + \boldsymbol{v}_1 \quad (12)$$

where $\boldsymbol{H}_1 = \begin{bmatrix} \boldsymbol{M}_2 & \boldsymbol{0}_{3 \times 9} & \boldsymbol{M}_1 \end{bmatrix}$, $\boldsymbol{0}_{3 \times 9}$ represents a zero matrix with 3 rows and 9 columns. $\boldsymbol{v}_1$ is the measurement noise.

The IMU position remains constant, and therefore, the theoretical velocity is zero. Taking the velocity error as the measurement, the measurement equation is given as

$$\boldsymbol{Z}_2 = \begin{bmatrix} \delta V_E & \delta V_N & \delta V_U \end{bmatrix}^T = \boldsymbol{H}_2 \boldsymbol{X} + \boldsymbol{v}_2 \quad (13)$$

where $\boldsymbol{H}_2 = \begin{bmatrix} \boldsymbol{0}_{3 \times 3} & \boldsymbol{I}_{3 \times 3} & \boldsymbol{0}_{3 \times 9} \end{bmatrix}$, $\boldsymbol{v}_2$ is the measurement noise.

Taking $\boldsymbol{Z}_1$ and $\boldsymbol{Z}_2$ together as the system measurement, the measurement equation is given as

$$\boldsymbol{Z}_k = \boldsymbol{H}_k \boldsymbol{X}_k + \boldsymbol{v}_k \quad (14)$$

where $\boldsymbol{Z}_k = \begin{bmatrix} \boldsymbol{Z}_1 \\ \boldsymbol{Z}_2 \end{bmatrix}$, $\boldsymbol{H}_k = \begin{bmatrix} \boldsymbol{H}_1 \\ \boldsymbol{H}_2 \end{bmatrix}$, $\boldsymbol{v}_k = \begin{bmatrix} \boldsymbol{v}_1 \\ \boldsymbol{v}_2 \end{bmatrix}$.

III. OBSERVABILITY ANALYSIS AND ROTATION SCHEME DESIGN

The observability analysis should be carried out first to ensure that the error parameters can be calibrated before performing the system-level calibration, and then the rotation scheme should be determined. In this work, the global observability analysis method [29], [30] has been employed to analyze the state vector to determine the state variables that can be observed.

$$\begin{aligned} \boldsymbol{Z}_1 &= \left[-\left(\boldsymbol{C}_b^{b_1} \boldsymbol{C}_n^b \boldsymbol{r}^n\right) \times\right] \boldsymbol{\mu} + \boldsymbol{C}_b^{b_1} \boldsymbol{C}_n^b \left(\boldsymbol{r}^n \times\right) \boldsymbol{\phi} \\ &= \begin{bmatrix} 0 & & -r_z^b \\ r_z^b & & 0 \\ \sin \psi_1 r_y^b - \cos \psi_1 r_x^b & & \cos \psi_1 r_x^b + \sin \psi_1 r_y^b \end{bmatrix} \end{aligned}$$

where, $\boldsymbol{C}_b^{b_1} = \begin{bmatrix} \cos \psi_1 & \sin \psi_1 & 0 \\ -\sin \psi_1 & \cos \psi_1 & 0 \\ 0 & 0 & 1 \end{bmatrix}$, $\boldsymbol{C}_n^b \boldsymbol{r}^n = \begin{bmatrix} r_x^b & r_y^b & r_z^b \end{bmatrix}^T$.

Owing to the field of view (FOV) being narrow, r_x^b and r_y^b are small, which makes the coefficient variation of $\boldsymbol{\mu}$ miniscule and cannot make the coupled error parameters optimally excited. Therefore, the rotation of other axes is also required to achieve the optimal excitation of the parameters.

A. Observability Analysis of Installation Error of Star Sensor

1) *Calibration of installation error of the NFOV star sensor*

In the calibration process, $\boldsymbol{Z}_1$ and its derivatives are known. According to the basic theory for solving linear equations, if there is a certain condition that causes the coefficient of an error parameter to change uncorrelatedly with the coefficients of other states, it is always possible to solve multiple sets of equations algebraically, so as to quantitatively calculate the analytical solution of the parameter. This implies that the parameter is observable under certain conditions. Concomitnaly, if the coefficient variation of the error parameter is larger, the estimated result will be less affected by the measurement noise and system noise, and the observability will be higher.

From (12), we get

$$\boldsymbol{Z}_1 = \left[-\left(\boldsymbol{C}_n^b \boldsymbol{r}^n\right) \times\right] \boldsymbol{\mu} + \boldsymbol{C}_n^b \left(\boldsymbol{r}^n \times\right) \boldsymbol{\phi} \quad (15)$$

where, $\boldsymbol{r}^n = \boldsymbol{C}_e^n \boldsymbol{r}^e$.

According to (15) the misalignment angle $\boldsymbol{\phi}$ and the star sensor installation error $\boldsymbol{\mu}$ are coupled. The coupling relationship can be understood as the coordinates of the starlight vector in the star sensor that are jointly affected by $\boldsymbol{\phi}$ and $\boldsymbol{\mu}$, and there are always different combinations of $\boldsymbol{\phi}$ and $\boldsymbol{\mu}$ to keep the coordinates unchanged. The decoupling method can be understood as the adoption of a certain way to make $\boldsymbol{\phi}$ and $\boldsymbol{\mu}$ uniquely determined.

As long as the coefficient matrices of $\boldsymbol{\phi}$ and $\boldsymbol{\mu}$ change uncorrelatedly, they can be separated from each other. The coefficient can be changed in two ways, one is to change $\boldsymbol{C}_n^m$ by changing the attitude of the IMU, and the other is to change $\boldsymbol{r}^n$ by the rotation of the earth or changing the starlight vector. Theoretically, both methods can separate $\boldsymbol{\phi}$ and $\boldsymbol{\mu}$, but owing to the small angular velocity of the Earth's rotation, the coefficient of the error parameter does not change significantly, thus making it difficult to separate $\boldsymbol{\phi}$ and $\boldsymbol{\mu}$. For NFOV star sensor, the starlight vector $\boldsymbol{r}^n$ changes very little, and there is even only one starlight vector, hence it can only be separated from $\boldsymbol{\phi}$ and $\boldsymbol{\mu}$ by changing the attitude of the IMU.

When the IMU is rotated by an angle ψ_1 around the z-axis, (15) becomes

$$\begin{bmatrix} -\sin \psi_1 r_y^b + \cos \psi_1 r_x^b \\ -\cos \psi_1 r_x^b - \sin \psi_1 r_y^b \\ 0 \end{bmatrix} \begin{bmatrix} \mu_x \\ \mu_y \\ \mu_z \end{bmatrix} + \boldsymbol{C}_b^{b_1} \boldsymbol{C}_n^b \left(\boldsymbol{r}^n \times\right) \boldsymbol{\phi} \quad (16)$$

Particularly, when the starlight vector coincides with the optical axis of the star sensor, (15) becomes

$$\boldsymbol{Z}_1 = \begin{bmatrix} 0 & -1 & 0 \\ 1 & 0 & 0 \\ 0 & 0 & 0 \end{bmatrix} \begin{bmatrix} \mu_x \\ \mu_y \\ \mu_z \end{bmatrix} + \boldsymbol{C}_n^b \left(\boldsymbol{r}^n \times\right) \boldsymbol{\phi} \quad (17)$$

According to (17), the coefficient of μ_z is zero at this time, which indicates that when the observed starlight vector is always aligned with the optical axis of the star sensor, μ_z cannot be observed even if the attitude of the IMU or the starlight

vector is changed. Therefore, it is necessary to avoid the starlight vector coinciding with the optical axis of the star sensor. It is applicable to the Kalman filter calibration method that employs either the vector as the measurement, or the elevation and azimuth angles as the measurement. Theoretically, the coefficients of μ_x, μ_y, and μ_z are at most 1 and at least -1. It requires that the angle between the starlight vector and the optical axis of the star sensor is $90°$, which is impossible. For a large change of the coefficient of $\boldsymbol{\mu}$, the angle between the starlight vector and the optical axis of the star sensor should be larger during the calibration process.

2) *Calibration of installation error of the Large field of view (LFOV) star sensor*

For the LFOV star sensor, there are multiple starlight vectors within the FOV. At this instance, $\boldsymbol{r}^n$ can be altered by changing the starlight vector. Although, by using the information of different starlight vectors in the same FOV can improve the observability of the parameters, the complete separation of $\boldsymbol{\phi}$ and $\boldsymbol{\mu}$ is not possible. Particularly, when the attitude of the IMU is the unit matrix, (15) becomes

$$\boldsymbol{Z}_1 = \begin{bmatrix} 0 & r_z^n & -r_y^n \\ -r_z^n & 0 & r_x^n \\ r_y^n & -r_x^n & 0 \end{bmatrix} \begin{bmatrix} \mu_x \\ \mu_y \\ \mu_z \end{bmatrix} + \begin{bmatrix} 0 & -r_z^n & r_y^n \\ r_z^n & 0 & -r_x^n \\ -r_y^n & r_x^n & 0 \end{bmatrix} \begin{bmatrix} \phi_E \\ \phi_N \\ \phi_U \end{bmatrix} \quad (18)$$

According to (18), the coefficients of $\boldsymbol{\phi}$ and $\boldsymbol{\mu}$ are related. Despite multiple starlight vectors being in the FOV, the observability of the parameters cannot be improved by replacing the starlight vectors. Similarly, when the attitude angle is $[i\times90° \; j\times90° \; k\times90°]$ $(i, j, k = 0, \pm1, \pm2)$, only one element of each row and column of matrix $\boldsymbol{C}_n^m$ is 1, whereas the other elements are zero. This makes the coefficients of $\boldsymbol{\phi}$ and $\boldsymbol{\mu}$ correlated, so that $\boldsymbol{\phi}$ and $\boldsymbol{\mu}$ are coupled and the observability cannot be improved by replacing the starlight vector. Therefore, for the LFOV star sensor, to improve the observability of the system by replacing the starlight vector at a single position, stopping at the position with the attitude angle $[i\times90° \; j\times90° \; k\times90°]$ $(i, j, k = 0, \pm1, \pm2)$ should be avoided.

B. Observability of IMU Error Parameters

Derivation of (10)

$$\begin{aligned} \dot{\boldsymbol{Z}}_1 &= \Delta\dot{\boldsymbol{r}}^s = \left((\boldsymbol{\mu}\times)\boldsymbol{C}_n^b\boldsymbol{C}_e^n\boldsymbol{C}_i^e\boldsymbol{r}^i\right)' - \left(\boldsymbol{C}_n^b(\boldsymbol{\phi}\times)\boldsymbol{C}_e^n\boldsymbol{C}_i^e\boldsymbol{r}^i\right)' \\ &= \boldsymbol{C}_n^b\left(\boldsymbol{\omega}_{ie}^n\times\right)\boldsymbol{r}^n\times\boldsymbol{\mu} + \left[\boldsymbol{C}_n^b\left(\left(\boldsymbol{\omega}_{ni}^n\times\right)\boldsymbol{r}^n\times\right) - \left(\boldsymbol{C}_n^b\left(\boldsymbol{\omega}_{ni}^n\times\right) + \left(\boldsymbol{\omega}_{ib}^b\times\right)\boldsymbol{C}_n^b\right)\left(\boldsymbol{r}^n\times\right)\right]\boldsymbol{\phi} + \boldsymbol{C}_n^b\left(\boldsymbol{r}^n\times\right)\dot{\boldsymbol{\phi}} \\ &= \boldsymbol{C}_n^b\left(\boldsymbol{\omega}_{ie}^n\times\right)\boldsymbol{r}^n\times\boldsymbol{\mu} - \left[\boldsymbol{C}_n^b\left(\left(\boldsymbol{\omega}_{ni}^n\times\right)\boldsymbol{r}^n\times\right) - \left(\boldsymbol{C}_n^b\left(\boldsymbol{\omega}_{ni}^n\times\right) + \left(\boldsymbol{\omega}_{ib}^b\times\right)\boldsymbol{C}_n^b\right)\left(\boldsymbol{r}^n\times\right)\right]\boldsymbol{\phi} - \boldsymbol{C}_n^b\left(\boldsymbol{r}^n\times\right)\left[\boldsymbol{\omega}_{ie}^n\times\boldsymbol{\phi} + \boldsymbol{C}_b^n\left(\left(\boldsymbol{K}_g + \boldsymbol{K}_{gg}\right)\boldsymbol{\omega}_{ib}^b - \boldsymbol{\varepsilon}^b\right) - \delta\boldsymbol{\omega}_{in}^n\right] \end{aligned} \quad (19)$$

It can be seen from (19) that the gyro error parameters are hidden in the derivative of the measurement equation, though all the coefficients contain $\boldsymbol{C}_n^b(\boldsymbol{r}^n\times)$, which indicates that the error parameters cannot be separated from each other by changing the starlight vector, and can only be separated by the IMU rotation. Thus the estimation of the gyro error parameters depends only on the attitude error equation. The parameter $\boldsymbol{\phi}$ can be directly estimated through (12), though the starlight vector cannot be used as a measurement to directly observe the IMU error parameters. Without the measurement information

of the star sensor, $\boldsymbol{\phi}$ can only be estimated by the velocity error equation. However, in the velocity error equation, $\boldsymbol{\phi}$ is coupled with several state quantities, which complicates the segregation of the error parameters, especially ϕ_U. Therefore, the addition of the measurement information of the star sensor as the measurement is more conducive for the estimation of the gyro error parameters.

Taking the velocity as the measurement, then $\delta\boldsymbol{V}^n$ and its derivatives are known, and the velocity error equation can be written as

$$\begin{aligned} \dot{\boldsymbol{Z}} &= \delta\dot{\boldsymbol{V}}^n = -\boldsymbol{\phi}^n\times\boldsymbol{f}^n + \boldsymbol{C}_b^n\left[\left(\delta\boldsymbol{K}_a + \delta\boldsymbol{K}_{aa}\right)\boldsymbol{f}^b + \nabla^b\right] + \delta\boldsymbol{V}^n\times\left(2\boldsymbol{\omega}_{ie}^n + \boldsymbol{\omega}_{en}^n\right) + \boldsymbol{V}^n\times\left(2\delta\boldsymbol{\omega}_{ie}^n + \delta\boldsymbol{\omega}_{en}^n\right) \\ &= \begin{bmatrix} 0 & \phi_U & -\phi_N \\ -\phi_U & 0 & \phi_E \\ \phi_N & -\phi_E & 0 \end{bmatrix} \begin{bmatrix} 0 \\ 0 \\ g \end{bmatrix} + \boldsymbol{C}_b^n\left(\begin{bmatrix} \delta K_{ax} & 0 & 0 \\ \delta K_{ayx} & \delta K_{ay} & 0 \\ \delta K_{azx} & \delta K_{azy} & \delta K_{az} \end{bmatrix} \begin{bmatrix} f_x \\ f_y \\ f_z \end{bmatrix} + \begin{bmatrix} \nabla_x \\ \nabla_y \\ \nabla_z \end{bmatrix}\right) + \delta\boldsymbol{V}^n\times\left(2\boldsymbol{\omega}_{ie}^n + \boldsymbol{\omega}_{en}^n\right) + \boldsymbol{V}^n\times\left(2\delta\boldsymbol{\omega}_{ie}^n + \delta\boldsymbol{\omega}_{en}^n\right) \end{aligned} \quad (20)$$

According to (20), a reasonable change of the attitude of the IMU can induce uncorrelated changes in the coefficients of $\delta\boldsymbol{K}_a$, $\delta\boldsymbol{K}_{aa}$, and ∇^b, so that the error parameters can be separated from each other and improve their observability. To obtain the best observation, the change of the coefficient should be the largest. The maximum variation of the coefficients of $\delta\boldsymbol{K}_{aa}$, $\delta\boldsymbol{K}_a$, and ∇^b is 2g, g, and 2, respectively. To complete the optimal excitation of all the parameters in $\delta\boldsymbol{K}_a$ and $\delta\boldsymbol{K}_{aa}$, the axes x, y, and z of the

IMU must have the same and opposite processes as the direction of gravity. By rotating $180°$ around the axis that does not coincide with the direction of gravity, the accelerometer constant bias of the remaining two axes can be optimally excited. Therefore, it takes at least 5 rotations to determine the optimal excitation of the accelerometer error parameters.

The attitude error equation is given below.

$$\begin{aligned} \dot{\boldsymbol{\phi}}^n &= -\boldsymbol{\omega}_{ie}^n\times\boldsymbol{\phi}^n - \boldsymbol{C}_m^n\delta\boldsymbol{\omega}_{ib}^b + \delta\boldsymbol{\omega}_{in}^n = -\boldsymbol{\omega}_{ie}^n\times\boldsymbol{\phi}^n - \boldsymbol{C}_b^n\left[\left(\delta\boldsymbol{K}_g + \delta\boldsymbol{K}_{gg}\right)\boldsymbol{\omega}_{ib}^b - \boldsymbol{\varepsilon}^b\right] + \delta\boldsymbol{\omega}_{in}^n \\ &= \begin{bmatrix} 0 & \omega_{ie}\sin L & -\omega_{ie}\cos L \\ -\omega_{ie}\sin L & 0 & 0 \\ \omega_{ie}\cos L & 0 & 0 \end{bmatrix} \begin{bmatrix} \phi_E \\ \phi_N \\ \phi_U \end{bmatrix} - \boldsymbol{C}_b^n\left(\begin{bmatrix} \delta K_{gx} & \delta K_{gxy} & \delta K_{gxz} \\ \delta K_{gyx} & \delta K_{gy} & \delta K_{gyz} \\ \delta K_{gzx} & \delta K_{gzy} & \delta K_{gz} \end{bmatrix} \begin{bmatrix} \omega_x \\ \omega_y \\ \omega_z \end{bmatrix} - \begin{bmatrix} \varepsilon_x \\ \varepsilon_y \\ \varepsilon_z \end{bmatrix}\right) + \delta\boldsymbol{\omega}_{in}^n \end{aligned} \quad (21)$$

According to (21), after ϕ is observed, all the three axes x, y, and z, of the IMU need to be rotated for an uncorrelated change of the coefficients of the error parameters in δK_{gg} and δK_g, and hence to excite each error parameter. The maximum variation of the coefficient of δK_{gg} is 2ω. Here ω is the rotational angular velocity of the IMU. If the coefficient contains $\sin(\omega t)$, it needs to be rotated by $270°$. If the coefficient contains $\cos(\omega t)$, it needs to be rotated by $180°$. Since δK_g is on the main diagonal, it is necessary to rotate the IMU forward and reverse, or depend on the change of C_m^n to make its coefficient ω change in the opposite direction. Furthermore, if ω does not change during the rotation, the coefficients of δK_{gg} and δK_g and the coefficient of ε^b will have correlated change, which will be detrimental to the separation of δK_{gg}, δK_g and ε^b. However, ε^b can be ignored since it is negligible when compared to δK_{gg} and δK_g. Further, in the actual rotation process, ω will inevitably go through an acceleration and deceleration process, hence the condition will be satisfied in the actual calibration process. The calibration of ε^b is performed when the IMU is stationary.

The attitude error equation when the IMU is stationary can be given as

$$\dot{\phi}^n = \omega_{ie}\begin{bmatrix} \sin L\phi_N - \cos L\phi_U \\ -\sin L\phi_E \\ \cos L\phi_E \end{bmatrix} - C_{b0}^n C_{b1}^{b0}\left(\begin{bmatrix} \delta K_{gx} & \delta K_{gxy} & \delta K_{gxz} \\ \delta K_{gyx} & \delta K_{gy} & \delta K_{gyz} \\ \delta K_{gzx} & \delta K_{gzy} & \delta K_{gz} \end{bmatrix} C_{b0}^{b1} C_n^{b0}\begin{bmatrix} 0 \\ \omega_{ie}\cos L \\ \omega_{ie}\sin L \end{bmatrix} - \begin{bmatrix} \varepsilon_x \\ \varepsilon_y \\ \varepsilon_z \end{bmatrix}\right) + \delta\omega_{in}^n \tag{22}$$

where $C_{b_0}^n$ is the attitude matrix before rotation, and $C_{b_1}^{b_0}$ is the b-frame transformation matrix before and after the rotation. According to (22), ω_{ie} will affect the estimation accuracy of ε^b. Assuming that the attitude matrix at the initial moment is a unit matrix, ε^b will be coupled with an installation error and a scale factor error as long as the IMU rotates at an integral multiple of $90°$ no matter where it stops. Taking the attitude error equation on the north direction as an example, the estimation accuracy of ε_x has been analyzed.

$$\dot{\phi}_N = -\omega_{ie}\sin L\phi_E - \omega_{ie}\cos L\delta K_{gx} + \omega_{ie}\sin L\delta K_{gxz} - \varepsilon_x + \delta\omega_{inN}^n \tag{23}$$

Assuming that the latitude of the calibration location is $45°$N, the gyro installation error is $30''$, and the scale factor error is 60 ppm. Therefore, the maximum error caused by ω_{ie} is 1.059×10^{-8} rad/s, and the minimum error is 4.406×10^{-9} rad/s. If the constant drift of the gyro is 0.005 °/h when the induced error is the maximum, the estimated error will reach 43.7%, which is unacceptable for calibration. The error caused by ω_{ie} needs be minimized, and the estimated error is 18.2%. However, the positive and negative values of the installation error cannot be determined before the calibration. Therefore, the positive and negative coefficients should have the same and opposite cases while designing the rotation scheme. For a better estimate, the coefficients of ε^b need to undergo largest uncorrelated changes so that ε^b are completely separated from the other quantities.

According to (22), two conditions must be satisfied for the coefficient of ε^b to have a maximum uncorrelated change. One is to change the sign of ε^b, while the corresponding equation remains unchanged. The second is to keep the coefficients of δK_{gg} and δK_g unchanged, while keeping the correponding equation unchanged. First, change the sign of ε^b, i.e., IMU is rotated $180°$, or by an odd multiple of $180°$, around an axis. Accordingly, the signs of ε^b of the other two axes can be changed in the opposite direction and ensure that they are contained in the original equation. To keep the coefficients of δK_{gg} and δK_g unchanged, the sign of the variables in $C_n^{b_0}[0, \omega_{ie}\cos L, \omega_{ie}\sin L]^T$ needs to change. This implies that there is only one rotation that meets the requirements, i.e., the IMU rotated by $180°$, or by an odd multiple of $180°$, around the axis where the ω_{ie} component in the b-frame is zero.

C. Rotation Scheme Design

Since ω_{ie}^n, ω_{en}^n, $\delta\omega_{ie}^n$, $\delta\omega_{en}^n$, and $\delta\omega_{in}^n$ do not affect the observability of the system, they are omitted from the observability analysis for the sake of brevity.

Assuming that the b-frame and n-frame coincide at the initial moment

$$\delta\dot{V}^n = \begin{bmatrix} -\phi_N g \\ \phi_E g \\ 0 \end{bmatrix} + \begin{bmatrix} \nabla_x \\ \nabla_y \\ \nabla_z + f_z\delta K_{az} \end{bmatrix} = \begin{bmatrix} -\phi_N g \\ \phi_E g \\ 0 \end{bmatrix} + \begin{bmatrix} \nabla_x \\ \nabla_y \\ g\delta K_{az} + \nabla_z \end{bmatrix} \tag{24}$$

$$\dot{\phi}^n = \omega_{ie}\begin{bmatrix} \sin L\phi_N - \cos L\phi_U \\ -\sin L\phi_E \\ \cos L\phi_E \end{bmatrix} - \begin{bmatrix} \omega_{ie}\cos L\delta K_{gxy} + \omega_{ie}\sin L\delta K_{gxz} - \varepsilon_x \\ \omega_{ie}\cos L\delta K_{gy} + \omega_{ie}\sin L\delta K_{gyz} - \varepsilon_y \\ \omega_{ie}\cos L\delta K_{gzy} + \omega_{ie}\sin L\delta K_{gz} - \varepsilon_z \end{bmatrix} \tag{25}$$

According to (24) and (25), each error parameter is coupled with each other at this time.

1st rotation: The IMU rotates $180°$ around the y-axis

$$\delta\dot{V}^n = \begin{bmatrix} -\phi_N g \\ \phi_E g \\ 0 \end{bmatrix} + \begin{bmatrix} \cos(\omega t)\left(\nabla_x - \sin(\omega t)g\delta K_{ax}\right) + \sin(\omega t)\left(\nabla_z - \sin(\omega t)g\delta K_{azx} + \cos(\omega t)g\delta K_{az}\right) \\ \nabla_y - \sin(\omega t)g\delta K_{ayx} \\ -\sin(\omega t)\left(\nabla_x - \sin(\omega t)g\delta K_{ax}\right) + \cos(\omega t)\left(\nabla_z - \sin(\omega t)g\delta K_{azx} + \cos(\omega t)g\delta K_{az}\right) \end{bmatrix} \tag{26}$$

$$\dot{\phi}^n = \omega_{ie}\begin{bmatrix} \sin L\phi_N - \cos L\phi_U \\ -\sin L\phi_E \\ \cos L\phi_E \end{bmatrix} - \begin{bmatrix} \cos(\omega t)\left(\omega\delta K_{gxy} - \varepsilon_x\right) + \sin(\omega t)\left(\omega\delta K_{gzy} - \varepsilon_z\right) \\ \omega\delta K_{gy} - \varepsilon_y \\ -\sin(\omega t)\left(\omega\delta K_{gxy} - \varepsilon_x\right) + \cos(\omega t)\left(\omega\delta K_{gzy} - \varepsilon_z\right) \end{bmatrix} \tag{27}$$

According to (26) and (27), the rotation of the IMU makes the coefficient changes of ∇_x, ∇_z, δK_{ax}, δK_{az}, δK_{azx}, δK_{ayx}, δK_{gxy}, δK_{gzy}, and δK_{gy} uncorrelated. Hence they are separated from each other, and their observability is improved. The coefficients

of ∇_x, ∇_z, δK_{ax}, δK_{az}, δK_{gxy}, and δK_{gzy} have the largest uncorrelated changes, so that they are better observed. After ∇_x is observed, ϕ_N can be estimated efficiently.

When the IMU is stationary

$$\dot{\boldsymbol{\phi}}^n = \omega_{ie}\begin{bmatrix} \sin L\phi_N - \cos L\phi_U \\ -\sin L\phi_E \\ \cos L\phi_E \end{bmatrix} - \begin{bmatrix} -\omega_{ie}\cos L\delta K_{gxy} + \omega_{ie}\sin L\delta K_{gxz} + \varepsilon_x \\ \omega_{ie}\cos L\delta K_{gy} - \omega_{ie}\sin L\delta K_{gyz} - \varepsilon_y \\ -\omega_{ie}\cos L\delta K_{gzy} + \omega_{ie}\sin L\delta K_{gz} + \varepsilon_z \end{bmatrix}$$

(28)

$$\delta\dot{\boldsymbol{V}}^n = \begin{bmatrix} -\phi_N g \\ \phi_E g \\ 0 \end{bmatrix} + \begin{bmatrix} -\nabla_x \\ \cos(\omega t)(\nabla_y - g\sin(\omega t)\delta K_{ay}) - \sin(\omega t)(\nabla_z - g\sin(\omega t)\delta K_{azy} - g\cos(\omega t)\delta K_{az}) \\ -\sin(\omega t)(\nabla_y - g\sin(\omega t)\delta K_{ay}) - \cos(\omega t)(\nabla_z - g\sin(\omega t)\delta K_{azy} - g\cos(\omega t)\delta K_{az}) \end{bmatrix}$$

(29)

$$\dot{\boldsymbol{\phi}}^n = \omega_{ie}\begin{bmatrix} \sin L\phi_N - \cos L\phi_U \\ -\sin L\phi_E \\ \cos L\phi_E \end{bmatrix} - \begin{bmatrix} -\omega\delta K_{gx} + \varepsilon_x \\ \cos(\omega t)(\omega\delta K_{gyx} - \varepsilon_y) - \sin(\omega t)(\omega\delta K_{gzx} - \varepsilon_z) \\ -\sin(\omega t)(\omega\delta K_{gyx} - \varepsilon_y) - \cos(\omega t)(\omega\delta K_{gzx} - \varepsilon_z) \end{bmatrix}$$

(30)

According to (29) and (30), the rotation of the IMU makes the coefficient changes of ∇_y, ∇_z, δK_{ay}, δK_{az}, δK_{azy}, δK_{gx}, δK_{gyx}, and δK_{gzx} uncorrelated. Hence they are separated from each other, and their observability is improved. The coefficients of ∇_y, ∇_z, δK_{ay}, δK_{az}, δK_{gyx}, and δK_{gzx} have the largest uncorrelated changes, so that they are better observed. After ∇_y is observed, ϕ_E can be estimated more efficiently.

When the IMU is stationary

$$\delta\dot{\boldsymbol{V}}^n = \begin{bmatrix} -\phi_N g \\ \phi_E g \\ 0 \end{bmatrix} + \begin{bmatrix} -\cos(\omega t)(\nabla_x - \sin(\omega t)g\delta K_{ax}) - \sin(\omega t)(\nabla_z - \sin(\omega t)g\delta K_{azx} + \cos(\omega t)g\delta K_{az}) \\ -\nabla_y + \sin(\omega t)g\delta K_{ayx} \\ -\sin(\omega t)(\nabla_x - \sin(\omega t)g\delta K_{ax}) + \cos(\omega t)(\nabla_z - \sin(\omega t)g\delta K_{azx} + \cos(\omega t)g\delta K_{az}) \end{bmatrix}$$

(32)

$$\dot{\boldsymbol{\phi}}^n = \omega_{ie}\begin{bmatrix} \sin L\phi_N - \cos L\phi_U \\ -\sin L\phi_E \\ \cos L\phi_E \end{bmatrix} - \begin{bmatrix} -\cos(\omega t)(\omega\delta K_{gxy} - \varepsilon_x) - \sin(\omega t)(\omega\delta K_{gzy} - \varepsilon_z) \\ -\omega\delta K_{gy} + \varepsilon_y \\ -\sin(\omega t)(\omega\delta K_{gxy} - \varepsilon_x) + \cos(\omega t)(\omega\delta K_{gzy} - \varepsilon_z) \end{bmatrix}$$

(33)

According to (32) and (33), the rotation of the IMU makes the coefficient changes of ∇_x, ∇_z, δK_{ax}, δK_{az}, δK_{azx}, δK_{gxy}, δK_{gzy}, and δK_{gy} uncorrelated. Hence they are separated from each other, and their observability is improved. The coefficients of δK_{gy}, δK_{ax}, δK_{az}, and δK_{gy} have the largest uncorrelated changes, so that they are better observed.

When the IMU is stationary

$$\delta\dot{\boldsymbol{V}}^n = \begin{bmatrix} -\phi_N g \\ \phi_E g \\ 0 \end{bmatrix} + \begin{bmatrix} -\nabla_z + g\cos(\omega t)\delta K_{azx} - g\sin(\omega t)\delta K_{azy} \\ -\sin(\omega t)(\nabla_x - g\cos(\omega t)\delta K_{ax}) - \cos(\omega t)(\nabla_y - g\cos(\omega t)\delta K_{ayx} + g\sin(\omega t)\delta K_{ay}) \\ -\cos(\omega t)(\nabla_x - g\cos(\omega t)\delta K_{ax}) + \sin(\omega t)(\nabla_y - g\cos(\omega t)\delta K_{ayx} + g\sin(\omega t)\delta K_{ay}) \end{bmatrix}$$

(35)

$$\dot{\boldsymbol{\phi}}^n = \omega_{ie}\begin{bmatrix} \sin L\phi_N - \cos L\phi_U \\ -\sin L\phi_E \\ \cos L\phi_E \end{bmatrix} - \begin{bmatrix} -\omega\delta K_{gz} + \varepsilon_z \\ -\sin(\omega t)(\omega\delta K_{gxz} - \varepsilon_x) - \cos(\omega t)(\omega\delta K_{gyz} - \varepsilon_y) \\ -\cos(\omega t)(\omega\delta K_{gxz} - \varepsilon_x) + \sin(\omega t)(\omega\delta K_{gyz} - \varepsilon_y) \end{bmatrix}$$

(36)

According to (35) and (36), the rotation of the IMU makes the coefficient changes of ∇_x, ∇_y, δK_{ax}, δK_{ay}, δK_{azx}, δK_{azy}, δK_{ayx}, δK_{gz}, δK_{gxz}, and δK_{gyz} uncorrelated. Hence their observability is

According to (28), if the two error parameters coupled with ε^b have the same sign, the estimator of ε^b contains less error. Since ϕ_U is still relatively large, ε_z cannot be effectively estimated. Owing to the existence of $\omega_{ie}\cos L$, the magnitude of $\omega_{ie}\cos L\phi_U$ is small, hence ε_x can be observed. If the two error parameters that are coupled with ε^b have opposite signs, the estimator will contain a larger error. Therefore, it is necessary to design the rotation order that will produce different symbols.

2nd rotation: The IMU rotates 180° around the x-axis

$$\dot{\boldsymbol{\phi}}^n = \omega_{ie}\begin{bmatrix} \sin L\phi_N - \cos L\phi_U \\ -\sin L\phi_E \\ \cos L\phi_E \end{bmatrix} - \begin{bmatrix} \omega_{ie}\cos L\delta K_{gxy} - \omega_{ie}\sin L\delta K_{gxz} + \varepsilon_x \\ \omega_{ie}\cos L\delta K_{gy} - \omega_{ie}\sin L\delta K_{gy} + \varepsilon_y \\ -\omega_{ie}\cos L\delta K_{gzy} + \omega_{ie}\sin L\delta K_{gz} - \varepsilon_z \end{bmatrix}$$

(31)

According to (31), the coefficients of ε_y and ε_z have the largest uncorrelated changes, and their observability is improved.

3rd rotation: The IMU rotates 90° around the y-axis

$$\dot{\boldsymbol{\phi}}^n = \omega_{ie}\begin{bmatrix} \sin L\phi_N - \cos L\phi_U \\ -\sin L\phi_E \\ \cos L\phi_E \end{bmatrix} - \begin{bmatrix} \omega_{ie}\sin L\delta K_{gzx} + \omega_{ie}\cos L\delta K_{gzy} + \varepsilon_z \\ \omega_{ie}\sin L\delta K_{gyx} + \omega_{ie}\cos L\delta K_{gy} + \varepsilon_y \\ \omega_{ie}\sin L\delta K_{gx} + \omega_{ie}\cos L\delta K_{gxy} + \varepsilon_x \end{bmatrix}$$

(34)

According to (34), the coefficients of ε_x, ε_y, and ε_z do not change uncorrelatedly, hence their observability of the process cannot be improved.

4th rotation: The IMU rotates 180° around the z-axis

improved. The coefficients of ∇_x, ∇_y, δK_{ax}, δK_{ay}, δK_{azx}, δK_{gxz}, and δK_{gyz} have the largest uncorrelated changes, so that they are better observed.

When the IMU is stationary

$$
\dot{\boldsymbol{\phi}}^n = \omega_{ie}\begin{bmatrix} \sin L\phi_N - \cos L\phi_U \\ -\sin L\phi_E \\ \cos L\phi_E \end{bmatrix} - \begin{bmatrix} -\omega_{ie}\sin L\delta K_{gzx} - \omega_{ie}\cos L\delta K_{gzy} + \varepsilon_z \\ \omega_{ie}\sin L\delta K_{gyx} + \omega_{ie}\cos L\delta K_{gy} - \varepsilon_y \\ \omega_{ie}\sin L\delta K_{gx} + \omega_{ie}\cos L\delta K_{gxy} - \varepsilon_x \end{bmatrix}
\tag{37}
$$

$$
\delta\dot{\boldsymbol{V}}^n = \begin{bmatrix} -\phi_N g \\ \phi_E g \\ 0 \end{bmatrix} + \begin{bmatrix} \sin(\omega t)\big(g\cos(\omega t)\delta K_{ax} + \nabla_x\big) - \cos(\omega t)\big(g\cos(\omega t)\delta K_{azx} + g\sin(\omega t)\delta K_{az} + \nabla_z\big) \\ g\cos(\omega t)\delta K_{ayx} + \nabla_y \\ \cos(\omega t)\big(g\cos(\omega t)\delta K_{ax} + \nabla_x\big) + \sin(\omega t)\big(g\cos(\omega t)\delta K_{azx} + g\sin(\omega t)\delta K_{az} + \nabla_z\big) \end{bmatrix}
\tag{38}
$$

$$
\dot{\boldsymbol{\phi}}^n = \omega_{ie}\begin{bmatrix} \sin L\phi_N - \cos L\phi_U \\ -\sin L\phi_E \\ \cos L\phi_E \end{bmatrix} - \begin{bmatrix} \sin(\omega t)\big(\omega\delta K_{gxy} - \varepsilon_x\big) - \cos(\omega t)\big(\omega\delta K_{gzy} - \varepsilon_z\big) \\ \omega\delta K_{gy} - \varepsilon_y \\ \cos(\omega t)\big(\omega\delta K_{gxy} - \varepsilon_x\big) + \sin(\omega t)\big(\omega\delta K_{gzy} - \varepsilon_z\big) \end{bmatrix}
\tag{39}
$$

According to (38) and (39), the rotation of the IMU makes the coefficient changes of ∇_x, ∇_z, δK_{ax}, δK_{az}, δK_{azx}, δK_{ayx}, δK_{gxy}, δK_{gzy}, and δK_{gy} uncorrelated. Hence they are separated from each other, and their observability is improved. The coefficients of ∇_x, ∇_z, δK_{ax}, δK_{az}, δK_{ayx}, δK_{gxy}, δK_{gzy}, and δK_{gy} have the largest uncorrelated changes, so that they are better observed.

When the IMU is stationary

According to (37), the coefficients of ε_x and ε_y have the largest uncorrelated changes, hence their observability is improved.

5th rotation: The IMU rotates 180 °around the y-axis

$$
\dot{\boldsymbol{\phi}}^n = \omega_{ie}\begin{bmatrix} \sin L\phi_N - \cos L\phi_U \\ -\sin L\phi_E \\ \cos L\phi_E \end{bmatrix} - \begin{bmatrix} -\omega_{ie}\sin L\delta K_{gzx} + \omega_{ie}\cos L\delta K_{gzy} - \varepsilon_z \\ -\omega_{ie}\sin L\delta K_{gyx} + \omega_{ie}\cos L\delta K_{gy} - \varepsilon_y \\ \omega_{ie}\sin L\delta K_{gx} - \omega_{ie}\cos L\delta K_{gxy} + \varepsilon_x \end{bmatrix}
\tag{40}
$$

By comparing (40) with (37), the signs of the two error parameters coupled with $\boldsymbol{\varepsilon}^b$ are found to be opposite in one equation. The coupling error is reduced, thereby improving the estimation accuracy of $\boldsymbol{\varepsilon}^b$.

6th rotation: The IMU rotates 90 °around the z-axis

$$
\delta\dot{\boldsymbol{V}}^n = \begin{bmatrix} -\phi_N g \\ \phi_E g \\ 0 \end{bmatrix} + \begin{bmatrix} -g\cos(\omega t)\delta K_{azx} + g\sin(\omega t)\delta K_{azy} + \nabla_z \\ \sin(\omega t)\big(-g\cos(\omega t)\delta K_{ax} + \nabla_x\big) + \cos(\omega t)\big(-g\cos(\omega t)\delta K_{ayx} + g\sin(\omega t)\delta K_{ay} + \nabla_y\big) \\ -\cos(\omega t)\big(-g\cos(\omega t)\delta K_{ax} + \nabla_x\big) + \sin(\omega t)\big(-g\cos(\omega t)\delta K_{ayx} + g\sin(\omega t)\delta K_{ay} + \nabla_y\big) \end{bmatrix}
\tag{41}
$$

$$
\dot{\boldsymbol{\phi}}^n = \omega_{ie}\begin{bmatrix} \sin L\phi_N - \cos L\phi_U \\ -\sin L\phi_E \\ \cos L\phi_E \end{bmatrix} - \begin{bmatrix} \omega\delta K_{gz} - \varepsilon_z \\ \sin(\omega t)\big(\omega\delta K_{gxz} - \varepsilon_x\big) + \cos(\omega t)\big(\omega\delta K_{gyz} - \varepsilon_y\big) \\ -\cos(\omega t)\big(\omega\delta K_{gxz} - \varepsilon_x\big) + \sin(\omega t)\big(\omega\delta K_{gyz} - \varepsilon_y\big) \end{bmatrix}
\tag{42}
$$

According to (41) and (42), the rotation of the IMU makes the coefficient changes of ∇_x, ∇_y, δK_{ax}, δK_{ay}, δK_{ayx}, δK_{azx}, δK_{azy}, δK_{gz}, δK_{gxz}, and δK_{gyz} uncorrelated, hence their observability is improved. The coefficients of δK_{ax}, δK_{ay} δK_{azx}, and δK_{gz} have the largest uncorrelated changes, so that they are better observed.

When the IMU is stationary

$$
\dot{\boldsymbol{\phi}}^n = \omega_{ie}\begin{bmatrix} \sin L\phi_N - \cos L\phi_U \\ -\sin L\phi_E \\ \cos L\phi_E \end{bmatrix} - \begin{bmatrix} \omega_{ie}\cos L\delta K_{gzx} + \omega_{ie}\sin L\delta K_{gzy} - \varepsilon_z \\ \omega_{ie}\cos L\delta K_{gx} + \omega_{ie}\sin L\delta K_{gxy} - \varepsilon_x \\ \omega_{ie}\cos L\delta K_{gyx} + \omega_{ie}\sin L\delta K_{gy} - \varepsilon_y \end{bmatrix}
\tag{43}
$$

According to (43), the coefficient of ε_z has the largest uncorrelated change, hence it is better observed.

7th rotation: The IMU rotates 180 °around the x-axis

$$
\delta\dot{\boldsymbol{V}}^n = \begin{bmatrix} -\phi_N g \\ \phi_E g \\ 0 \end{bmatrix} + \begin{bmatrix} \sin(\omega t)\big(\cos(\omega t)g\delta K_{ay} + \nabla_y\big) + \cos(\omega t)\big(\cos(\omega t)g\delta K_{azy} - \sin(\omega t)g\delta K_{az} + \nabla_z\big) \\ \nabla_x \\ \cos(\omega t)\big(\cos(\omega t)g\delta K_{ay} + \nabla_y\big) - \sin(\omega t)\big(\cos(\omega t)g\delta K_{azy} - \sin(\omega t)g\delta K_{az} + \nabla_z\big) \end{bmatrix}
\tag{44}
$$

$$
\dot{\boldsymbol{\phi}}^n = \omega_{ie}\begin{bmatrix} \sin L\phi_N - \cos L\phi_U \\ -\sin L\phi_E \\ \cos L\phi_E \end{bmatrix} - \begin{bmatrix} \sin(\omega t)\big(\omega\delta K_{gyx} - \varepsilon_y\big) + \cos(\omega t)\big(\omega\delta K_{gzx} - \varepsilon_z\big) \\ \omega\delta K_{gx} - \varepsilon_x \\ \cos(\omega t)\big(\omega\delta K_{gyx} - \varepsilon_y\big) - \sin(\omega t)\big(\omega\delta K_{gzx} - \varepsilon_z\big) \end{bmatrix}
\tag{45}
$$

According to (44) and (45), the rotation of the IMU makes the coefficient changes of ∇_y, ∇_z, δK_{ay}, δK_{az}, δK_{azy}, δK_{gx}, δK_{gyz}, and δK_{gzx} uncorrelated, hence their observability is improved. The coefficients of ∇_y, ∇_z, δK_{ay}, δK_{az}, and δK_{gzx} have the largest uncorrelated change, so that they are better observed.

When the IMU is stationary

$$
\dot{\boldsymbol{\phi}}^n = \omega_{ie}\begin{bmatrix} \sin L\phi_N - \cos L\phi_U \\ -\sin L\phi_E \\ \cos L\phi_E \end{bmatrix} - \begin{bmatrix} -\omega_{ie}\cos L\delta K_{gzx} + \omega_{ie}\sin L\delta K_{gzy} + \varepsilon_z \\ \omega_{ie}\cos L\delta K_{gx} - \omega_{ie}\sin L\delta K_{gxy} - \varepsilon_x \\ -\omega_{ie}\cos L\delta K_{gyx} + \omega_{ie}\sin L\delta K_{gy} + \varepsilon_y \end{bmatrix}
\tag{46}
$$

Following the comparison of (46) with (43), the signs of the two error parameters coupled with $\boldsymbol{\varepsilon}^b$ must be opposite in one equation. The coupling error is reduced, thereby improving the estimation accuracy of $\boldsymbol{\varepsilon}^b$.

8th rotation: The IMU rotates 180 ° around the z-axis

$$\delta\dot{\boldsymbol{V}}^n = \begin{bmatrix} -\phi_N g \\ \phi_E g \\ 0 \end{bmatrix} + \begin{bmatrix} g\sin(\omega t)\delta K_{azx} + g\cos(\omega t)\delta K_{azy} - \nabla_z \\ \cos(\omega t)\left(-g\sin(\omega t)\delta K_{ax} + \nabla_x\right) - \sin(\omega t)\left(-g\sin(\omega t)\delta K_{ayx} - g\cos(\omega t)\delta K_{ay} + \nabla_y\right) \\ -\sin(\omega t)\left(-g\sin(\omega t)\delta K_{ax} + \nabla_x\right) - \cos(\omega t)\left(-g\sin(\omega t)\delta K_{ayx} - g\cos(\omega t)\delta K_{ay} + \nabla_y\right) \end{bmatrix} \quad (47)$$

$$\dot{\boldsymbol{\phi}}^n = \omega_{ie}\begin{bmatrix} \sin L\phi_N - \cos L\phi_U \\ -\sin L\phi_E \\ \cos L\phi_E \end{bmatrix} - \begin{bmatrix} -\omega\delta K_{gz} + \varepsilon_z \\ \cos(\omega t)\left(\omega\delta K_{gxz} - \varepsilon_x\right) - \sin(\omega t)\left(\omega\delta K_{gyz} - \varepsilon_y\right) \\ -\sin(\omega t)\left(\omega\delta K_{gxz} - \varepsilon_x\right) - \cos(\omega t)\left(\omega\delta K_{gyz} - \varepsilon_y\right) \end{bmatrix} \quad (48)$$

According to (47) and (48), the rotation of the IMU makes the coefficient changes of ∇_x, ∇_y, δK_{ax}, δK_{ay}, δK_{azx}, δK_{azy}, δK_{ayx}, δK_{gz}, δK_{gxz}, and δK_{gyz} uncorrelated, hence their observability is further improved. The coefficients of ∇_x, ∇_y, δK_{ax}, δK_{ay}, δK_{azy}, δK_{gz}, δK_{gxz}, and δK_{gyz} have the largest uncorrelated changes, so that they are better observed.

When the IMU is stationary

$$\dot{\boldsymbol{\phi}}^n = \omega_{ie}\begin{bmatrix} \sin L\phi_N - \cos L\phi_U \\ -\sin L\phi_E \\ \cos L\phi_E \end{bmatrix} - \begin{bmatrix} \omega_{ie}\cos L\delta K_{gzx} - \omega_{ie}\sin L\delta K_{gzy} + \varepsilon_z \\ \omega_{ie}\cos L\delta K_{gx} - \omega_{ie}\sin L\delta K_{gxy} + \varepsilon_x \\ -\omega_{ie}\cos L\delta K_{gyx} + \omega_{ie}\sin L\delta K_{gy} - \varepsilon_y \end{bmatrix} \quad (49)$$

According to (49), the coefficients of ε_x and ε_y have the largest uncorrelated changes, hence their observability is further improved.

9th rotation: The IMU rotates $-90°$ around the x-axis

$$\delta\dot{\boldsymbol{V}}^n = \begin{bmatrix} -\phi_N g \\ \phi_E g \\ 0 \end{bmatrix} + \begin{bmatrix} -\sin(\omega t)\left(g\cos(\omega t)\delta K_{ay} + \nabla_y\right) - \cos(\omega t)\left(g\cos(\omega t)\delta K_{azy} - g\sin(\omega t)\delta K_{az} + \nabla_z\right) \\ -\nabla_x \\ \cos(\omega t)\left(g\cos(\omega t)\delta K_{ay} + \nabla_y\right) - \sin(\omega t)\left(g\cos(\omega t)\delta K_{azy} - g\sin(\omega t)\delta K_{az} + \nabla_z\right) \end{bmatrix} \quad (50)$$

$$\dot{\boldsymbol{\phi}}^n = \omega_{ie}\begin{bmatrix} \sin L\phi_N - \cos L\phi_U \\ -\sin L\phi_E \\ \cos L\phi_E \end{bmatrix} - \begin{bmatrix} -\sin(\omega t)\left(\omega\delta K_{gyx} - \varepsilon_y\right) - \cos(\omega t)\left(\omega\delta K_{gzx} - \varepsilon_z\right) \\ -\omega\delta K_{gx} + \varepsilon_x \\ \cos(\omega t)\left(\omega\delta K_{gyx} - \varepsilon_y\right) - \sin(\omega t)\left(\omega\delta K_{gzx} - \varepsilon_z\right) \end{bmatrix} \quad (51)$$

According to (50) and (51), the rotation of the IMU makes the coefficient changes of ∇_y, ∇_z, δK_{ay}, δK_{az}, δK_{azy}, δK_{gzx}, δK_{gx}, and δK_{gyx} uncorrelated, such that their observability is further improved, where the coefficients of δK_{ay}, δK_{az}, δK_{gx}, δK_{gzx}, and δK_{gyx} have the largest uncorrelated changes, so that they are better observed.

When the IMU is stationary

$$\dot{\boldsymbol{\phi}}^n = \omega_{ie}\begin{bmatrix} \sin L\phi_N - \cos L\phi_U \\ -\sin L\phi_E \\ \cos L\phi_E \end{bmatrix} - \begin{bmatrix} \omega_{ie}\cos L\delta K_{gyx} - \omega_{ie}\sin L\delta K_{gyz} + \varepsilon_y \\ -\omega_{ie}\cos L\delta K_{gx} + \omega_{ie}\sin L\delta K_{gxz} - \varepsilon_x \\ -\omega_{ie}\cos L\delta K_{gzx} + \omega_{ie}\sin L\delta K_{gz} - \varepsilon_z \end{bmatrix} \quad (52)$$

According to (34), the coefficients of ε_x, ε_y, and ε_z do not change uncorrelatedly, hence their observability of the process cannot be improved.

10th rotation: The IMU rotates 180 ° around the y-axis

$$\delta\dot{\boldsymbol{V}}^n = \begin{bmatrix} -\phi_N g \\ \phi_E g \\ 0 \end{bmatrix} + \begin{bmatrix} g\sin(\omega t)\delta K_{ayx} + \nabla_y \\ -\cos(\omega t)\left(g\sin(\omega t)\delta K_{ax} + \nabla_x\right) - \sin(\omega t)\left(g\sin(\omega t)\delta K_{azx} + g\cos(\omega t)\delta K_{az} + \nabla_z\right) \\ -\sin(\omega t)\left(g\sin(\omega t)\delta K_{ax} + \nabla_x\right) + \cos(\omega t)\left(g\sin(\omega t)\delta K_{azx} + g\cos(\omega t)\delta K_{az} + \nabla_z\right) \end{bmatrix} \quad (53)$$

$$\dot{\boldsymbol{\phi}}^n = \omega_{ie}\begin{bmatrix} \sin L\phi_N - \cos L\phi_U \\ -\sin L\phi_E \\ \cos L\phi_E \end{bmatrix} - \begin{bmatrix} \omega\delta K_{gy} - \varepsilon_y \\ -\cos(\omega t)\left(\omega\delta K_{gxy} - \varepsilon_x\right) - \sin(\omega t)\left(\omega\delta K_{gzy} - \varepsilon_z\right) \\ -\sin(\omega t)\left(\omega\delta K_{gxy} - \varepsilon_x\right) + \cos(\omega t)\left(\omega\delta K_{gzy} - \varepsilon_z\right) \end{bmatrix} \quad (54)$$

According to (53) and (54), the rotation of the IMU makes the coefficient changes of ∇_x, ∇_z, δK_{ax}, δK_{az}, δK_{ayx}, δK_{azx}, δK_{gy}, δK_{gxy}, and δK_{gzy} uncorrelated, such that their observability is further improved, where the coefficients of ∇_x, ∇_z, δK_{ax}, δK_{az}, δK_{gy}, δK_{gxy}, and δK_{gzy} have the largest uncorrelated changes, so that they are better observed.

When the IMU is stationary

$$\dot{\boldsymbol{\phi}}^n = \omega_{ie}\begin{bmatrix} \sin L\phi_N - \cos L\phi_U \\ -\sin L\phi_E \\ \cos L\phi_E \end{bmatrix} - \begin{bmatrix} \omega_{ie}\cos L\delta K_{gyx} - \omega_{ie}\sin L\delta K_{gyz} - \varepsilon_y \\ \omega_{ie}\cos L\delta K_{gx} - \omega_{ie}\sin L\delta K_{gxz} - \varepsilon_x \\ -\omega_{ie}\cos L\delta K_{gzx} + \omega_{ie}\sin L\delta K_{gz} + \varepsilon_z \end{bmatrix} \quad (55)$$

According to (55), the coefficients of ε_y and ε_z have the largest uncorrelated changes, so that their observability is further improved.

According to the above analysis, the coefficients of each error parameter have the largest uncorrelated changes for the rotation scheme shown in Table I. Therefore, the error parameters can be optimally observed in fewer rotations.

TABLE I
ROTATION SCHEME FOR SYSTEM-LEVEL CALIBRATION

Sequence	Rotation degree and axis	Posture before rotation		
		X_b	Y_b	Z_b
1	$+180/Y_m$	East	North	Up
2	$+180/X_m$	West	North	Down
3	$+90/Y_m$	West	South	Up
4	$+180/Z_m$	Down	South	West
5	$+180/Y_m$	Up	North	West
6	$+90/Z_m$	Down	North	East
7	$+180/X_m$	North	Up	East
8	$+180/Z_m$	North	Down	West
9	$-90/X_m$	South	East	Up
10	$+180/Y_m$	North	East	Down

IV. SIMULATION AND EXPERIMENTS

A. Simulation Results and Analysis

The effectiveness of the above scheme has been verified by simulation. The calibration location is 109.3°E, 34.2°N, and the elevation is 400m. The initial attitude angle and velocity are both zero, and the simulation time is 1500s. The IMU sampling frequency is 100Hz. The random error of the gyro is $0.001°/\sqrt{h}$ and the random error of the accelerometer is $5\mu g/\sqrt{Hz}$. The standard deviation of the first-order Markov process of gyro and accelerometer is $0.001°/h$ and $5\mu g$, respectively, and the correlation time is 3600s. The measurement accuracy of the star sensor is 3" (1σ), and the update frequency 1Hz.

Both the traditional and proposed methods have been employed for the calibration. The traditional method is to calibrate the IMU error parameter and the star sensor installation error, separately. The proposed method employs the rotation scheme of Table I, and the rotation rate is set to 15 °/s, where each position remains stationary for 100s. A total of six simulations have been carried out, and the estimated curve of a single simulation is displayed in Fig. 2, and the preset value of the error parameter and the statistical feature quantity of the estimated value are listed in Table II. We observed that all the parameters in the proposed method can converge within 1500s, and both the estimation accuracy and stability are better than the traditional calibration method. It demonstrates the feasibility and effectiveness of the proposed calibration method.

To verify the correctness of the theoretical analysis, the angle between the starlight vector and the optical axis of the star sensor is set within the range of 30″, 1′, 30′, 1°, 2°, and 3° respectively for calibration. The mean value of the calibration results of the installation error of the six simulations is listed in Table III. We observed that the estimation accuracy of μ_z is higher for a larger the angle between the starlight vector and the optical axis of the star sensor. Therefore, in the calibration process, a small angle should be avoided.

TABLE II
STATISTICAL CHARACTERISTIC QUANTITIES OF STATE QUANTITY ESTIMATION RESIDUALS

Error coefficients	Preset value	Traditional method			Proposed method		
		Mean	Error	STD	Mean	Error	STD
ε_x (°/h)	0.005	0.00380	0.00120	0.00268	**0.00507**	**0.00048**	**0.00142**
ε_y (°/h)	0.005	0.00312	0.00188	0.00285	**0.00406**	**0.00094**	**0.00143**
ε_z (°/h)	0.005	0.00653	0.00153	0.00202	**0.00579**	**0.00079**	**0.00152**
δK_{gx} (ppm)	20	19.731	0.269	0.7394	**19.884**	**0.116**	**0.5873**
δK_{gy} (ppm)	40	40.795	0.795	0.8297	**39.619**	**0.381**	**0.6600**
δK_{gz} (ppm)	60	59.175	0.825	0.5611	**59.514**	**0.486**	**0.5958**
δK_{gxy} (″)	10	9.124	0.876	0.3588	**10.870**	**0.870**	**0.3371**
δK_{gxz} (″)	20	19.582	0.418	0.2780	**19.851**	**0.149**	**0.1756**
δK_{gyx} (″)	30	30.481	0.481	0.1800	**29.744**	**0.256**	**0.1838**
δK_{gyz} (″)	40	40.794	0.794	0.5615	**40.134**	**0.134**	**0.1582**
δK_{gzx} (″)	50	49.713	0.287	0.2847	**50.122**	**0.122**	**0.1156**
δK_{gzy} (″)	60	60.369	0.369	0.2489	**59.798**	**0.202**	**0.1991**
∇_x (μg)	20	18.644	1.356	3.2345	**18.763**	**1.237**	**2.0943**
∇_y (μg)	20	18.225	1.778	5.0499	**18.964**	**1.036**	**4.5046**
∇_z (μg)	20	21.749	1.749	4.5967	**20.565**	**0.565**	**2.8187**
δK_{ax} (ppm)	20	27.052	7.052	1.3422	**22.304**	**2.304**	**0.2581**
δK_{ay} (ppm)	40	43.745	3.745	0.9125	**42.324**	**2.324**	**0.2663**
δK_{az} (ppm)	60	64.956	4.956	0.9563	**61.020**	**1.020**	**0.9015**
δK_{ayx} (″)	20	19.540	0.460	0.4889	**20.445**	**0.445**	**0.3940**
δK_{azx} (″)	40	39.714	0.286	0.2066	**40.127**	**0.127**	**0.1558**
δK_{ayz} (″)	60	59.707	0.293	0.4707	**59.873**	**0.127**	**0.1707**
μ_x (″)	300	306.618	6.618	2.4587	**300.142**	**0.142**	**0.2258**
μ_y (″)	300	296.784	3.216	1.0138	**300.115**	**0.115**	**0.1174**
μ_z (″)	300	307.958	7.958	4.0121	**299.403**	**0.597**	**0.6457**

TABLE Ⅲ

ESTIMATION ACCURACY OF STAR SENSOR INSTALLATION ERROR AT DIFFERENT ANGLES

installation error	Preset value	30″	1′	30′	1°	2°	3°
μ_x (″)	300	300.041	300.107	300.105	299.997	300.153	300.086
μ_y (″)	300	300.114	300.012	299.951	300.048	299.999	300.121
μ_z (″)	300	234.316	264.316	292.304	297.126	298.891	299.631

(a) Gyro drifts

(b) Gyro scale factor errors

(c) Gyro installation errors

(d) Accelerometer biases

(e) Accelerometer scale factor errors

(f) Accelerometer installation errors

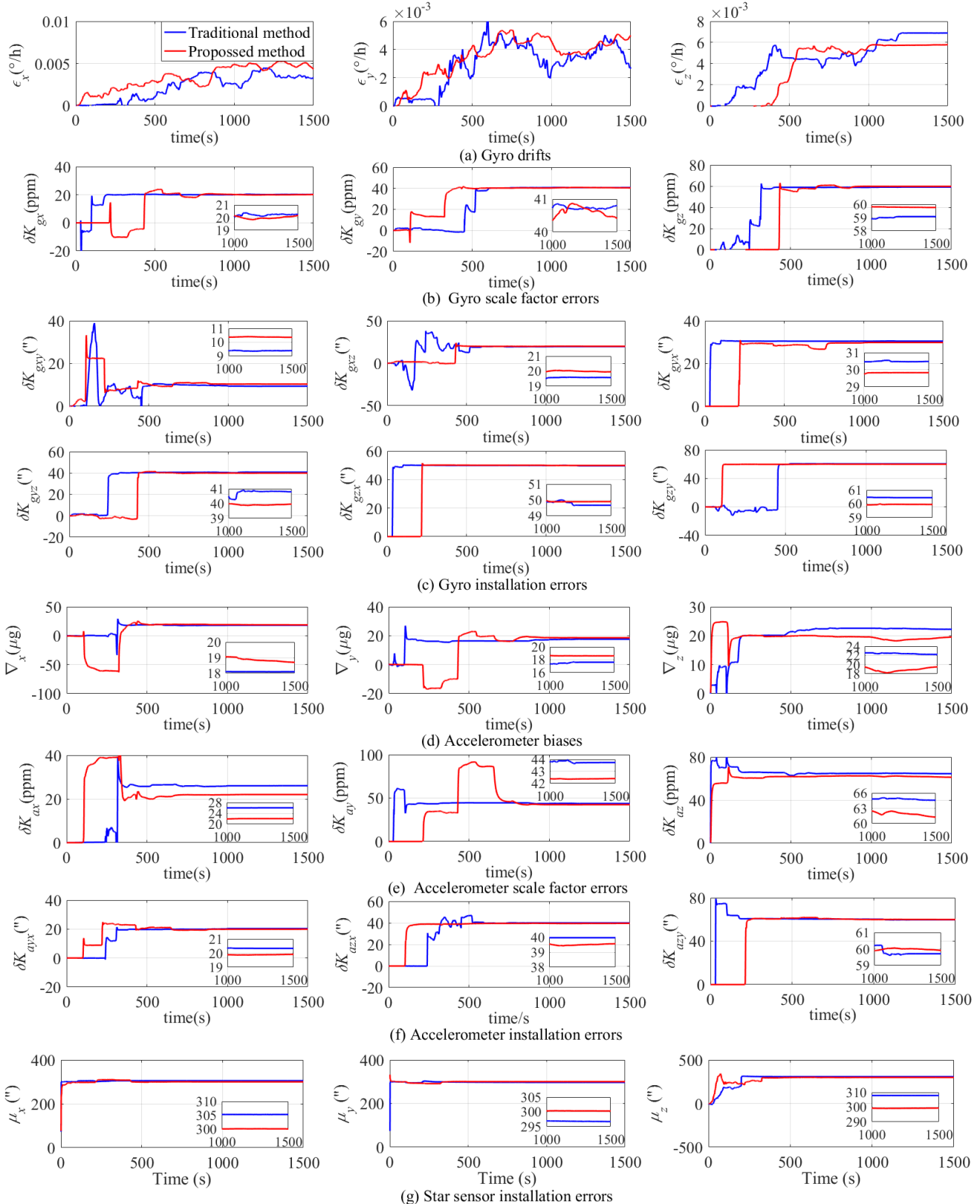(g) Star sensor installation errors

Fig. 2. Error parameter estimation curve.

In order to intuitively analyze the observability of the system, the covariance analysis method has been employed to analyze the observability of each error parameter. The mean square error matrix P_k of the standard Kalman filter reflects the covariance among the state variables. The diagonal element is the estimation error of the corresponding state quantity. The change of state estimation error can be seen from the change of P_k with time. Determine the observability of the jth state quantity as

$$\sigma_{k(j)} = \sqrt{\frac{P_{0(jj)}}{P_{k(jj)}}} \tag{56}$$

Where, $P_{0(jj)}$ is the element in row j and column j of the initial covariance matrix, and $P_{k(jj)}$ is the element in row j and column j of the covariance matrix at time k. The greater the value of $\sigma_{k(j)}$, the better the observability of the corresponding state quantity.

The observability of each error parameter is shown in Fig. 3. We observed that the observability of each error parameter shows different trends with the change of the IMU attitude. Overall, the observability of the star sensor installation error and accelerometer error parameters is higher, which shows the advantage of getting estimates directly from the measurement, and the observability of the constant drift is the lowest, which is consistent with the theoretical analysis. Following the Figs. 2 and 3, with the rotation of the IMU, the observability of the corresponding parameters is improved, and the estimation accuracy is also improved, which proves the correctness of the theoretical analysis.
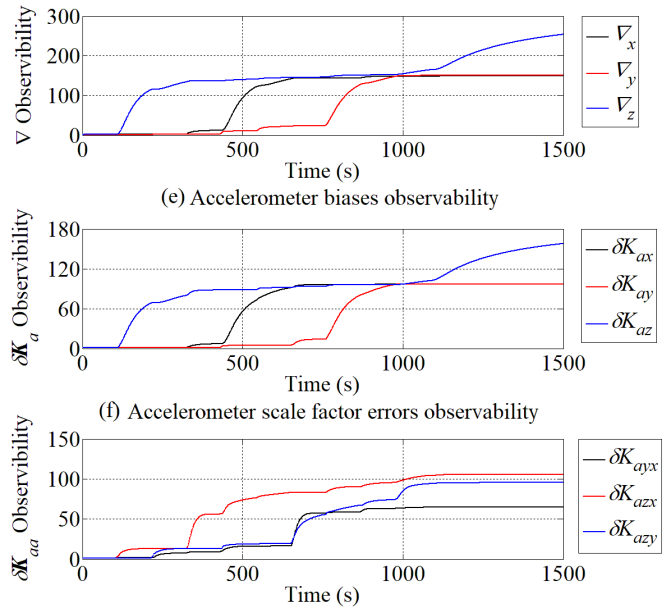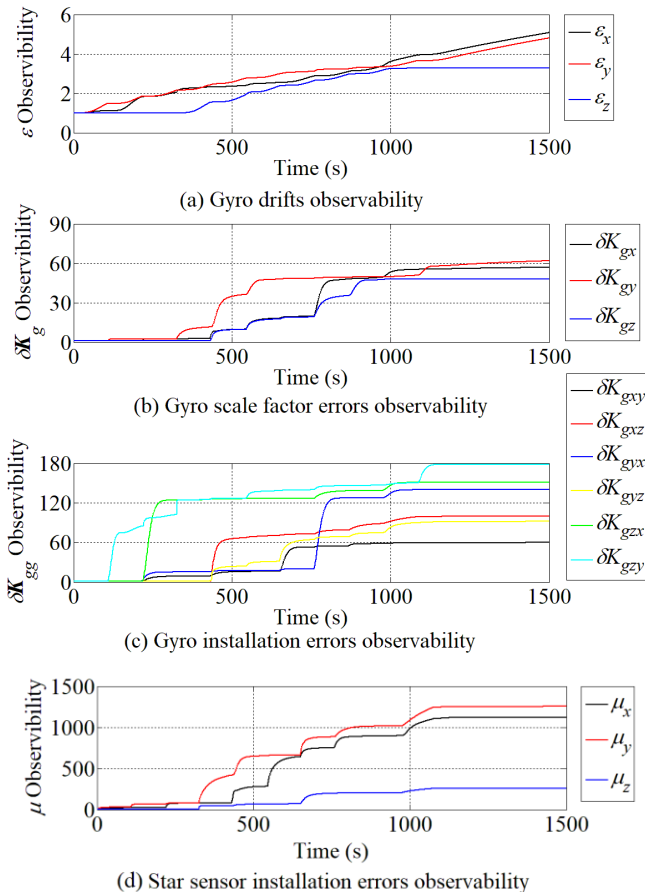

(a) Gyro drifts observability

(b) Gyro scale factor errors observability

(c) Gyro installation errors observability

(d) Star sensor installation errors observability

(e) Accelerometer biases observability

(f) Accelerometer scale factor errors observability

(g) Accelerometer installation errors observability

Fig. 3. Observability of the error parameters.

B. Experiment

To verify the performance of the algorithm, a ground calibration test has been carried out. The system consists of the star sensor, SINS, a turntable, three star simulators and a navigation computer. Three star simulators are mounted in the directions of east, west, and upward of the turntable, respectively. The star sensor has a measurement accuracy of 3.2"(1σ). Six experiments have been carried out using the traditional method and the proposed method. Table IV presents the calibration results of the two methods.

In Table IV, it is shown that the calibration results of the star sensor installation error of the two methods are quite different, whereas the differences of other error parameters are relatively small. However, the variance of the calibration results of the proposed method is significantly smaller than that of the traditional method, particularly, the installation error of the star sensor and the accelerometer scale factor. We observed that the proposed method can greatly improve the calibration stability and repeatability of the error parameters.

Repeated experiments cannot show the calibration accuracy of the proposed algorithm, hence the initial alignment method is employed to verify the accuracy of the calibration results. Since the calibrated error parameters include the inertial device error and the star sensor installation error, the initial alignment method adopted is the stellar-inertial alignment. The true value of the heading angle is given by a high-precision pendulum gyro north finder, with an accuracy of 2.8" (1σ), and the mean value of the measured heading angle is 1º12′27″. The results obtained by using the calibration results of the two methods for alignment are listed in Table V. We observed that the heading angle error is 13.1" while using the calibration results of the traditional calibration method for alignment, whereas the error is 3.4" for the calibration results of the proposed method. Thus the alignment accuracy has improved by about 74%, which proves that the proposed calibration method can significantly improve the navigation accuracy for practical applications.

TABLE IV

CALIBRATION RESULTS OF THE TWO METHODS

Error coefficients	Traditional method		Proposed method	
	Mean	STD	Mean	STD
ε_x (°/h)	0.00513	0.00178	**0.00607**	**0.00145**
ε_y (°/h)	0.00745	0.00392	**0.00856**	**0.00100**
ε_z (°/h)	0.00410	0.00185	**0.00531**	**0.00198**
δK_{gx} (ppm)	-11.421	0.8631	**-11.972**	**0.5384**
δK_{gy} (ppm)	12.134	1.2274	**11.957**	**0.4746**
δK_{gz} (ppm)	25.443	0.8546	**25.110**	**0.5791**
δK_{gxy} (″)	-107.589	1.7410	**-106.324**	**0.6152**
δK_{gxz} (″)	-113.596	1.8435	**-112.839**	**0.5471**
δK_{gyx} (″)	116.002	1.7496	**115.756**	**1.2274**
δK_{gyz} (″)	99.565	1.0740	**100.185**	**0.4827**
δK_{gzx} (″)	129.124	0.5171	**129.988**	**0.0774**
δK_{gzy} (″)	-80.695	0.6839	**-79.955**	**0.4748**
∇_x (μg)	48.253	1.7495	**49.363**	**0.5749**
∇_y (μg)	42.264	2.0784	**43.956**	**0.4744**
∇_z (μg)	25.891	1.4784	**27.856**	**0.8531**
δK_{ax} (ppm)	30.627	11.4102	**34.339**	**2.8741**
δK_{ay} (ppm)	-46.754	7.6741	**-44.613**	**1.5967**
δK_{az} (ppm)	-17.774	4.7528	**-14.560**	**1.9217**
δK_{ayx} (″)	201.395	0.8642	**200.874**	**0.4897**
δK_{azx} (″)	-138.741	1.2745	**-137.749**	**0.9785**
δK_{azy} (″)	115.784	1.2745	**116.376**	**1.2894**
μ_x (″)	-183.895	9.5754	**-190.353**	**0.7864**
μ_y (″)	-179.851	13.6342	**-176.698**	**0.7643**
μ_z (″)	-172.244	14.2764	**-183.871**	**0.8865**

TABLE V

ALIGNMENT RESULTS OF THE TWO METHODS

	Mean (°)	STD(′)	Error(″)
Traditional method	1.22753	0.93	13.1
Proposed method	1.20844	0.94	3.4

V. CONCLUSION

We propose an all-parameter system-level calibration method for the SINS/CNS integrated navigation system. By employing the velocity and starlight vector as measurements, all error parameters can be optimally observed through a 10-order rotation scheme. The estimation of bias, scale factor, misalignments of IMU, and installation errors of the star sensor can be achieved through a single calibration. Concomitantly, the influence of the angle between the starlight vector and the optical axis of the star sensor on the calibration of the installation error of the star sensor has been obtained, which has a certain significance for the selection of the star point. The calibration and alignment results of the proposed method are superior to those of the traditional methods, thus proving its feasibility and effectiveness.

REFERENCES

[1] E. Akeila, Z. Salcic, and A. Swain, "Reducing low-cost INS error accumulation in distance estimation using self-resetting," IEEE Trans. Instrum. Meas., vol. 63, no. 1, pp. 177-184, Jan. 2014.

[2] W. Wu, X. Ning, and L. Liu, "New celestial assisted INS initial alignment method for lunar explorer," J. Syst. Eng. Electron., vol. 24, no. 1, pp. 108-117, Feb. 2013.

[3] J. Lu, M. Hu, Y. Yang, and M. Dai, "On-Orbit Calibration Method for Redundant IMU Based on Satellite Navigation & Star Sensor Information Fusion," IEEE Sensors J., vol. 20, no. 9, pp. 4530-4543, 2020.

[4] X. Ning and L. Liu, "A two-mode INS/CNS navigation method for lunar rovers," IEEE Trans. Instrum. Meas., vol. 63, no. 9, pp. 2170-2179, Sep.

[5] H. Naseri, and M. R. Homaeinezhad, "Improving measurement quality of a MEMS-based gyro-free inertial navigation system," Sensors and Actuators A:Physical, vol. 207, pp. 10-19, 2014.

[6] G. A. Aydemir, and A. Saranlı, "Characterization and calibration of MEMS inertial sensors for state and parameter estimation applications," Measurement, vol. 45, no. 5, pp. 1210-1225, 2012.

[7] J. Lu, C. Lei, S. Liang, and Y. Yang, "An All-Parameter System-Level Calibration for Stellar-Inertial Navigation System on Ground," IEEE Trans. Instrum. Meas., vol. 66, no. 8, pp. 2065-2073, 2017.

[8] J. Lu, S. Liang, and L. Yang, "Analytic coarse alignment and calibration for inertial navigation system on swaying base assisted by star sensor," IET Science, Measurement & Technology, vol. 12, no. 5, pp. 673-677, 2018.

[9] Q. Ren, B. Wang, Z. Deng, and M. Fu, "A multi-position self-calibration method for dual-axis rotational inertial navigation system," Sensors and Actuators A: Physical, vol. 219, pp. 24-31, 2014.

[10] T. Nieminen, J. Kangas, S. Suuriniemi, and L. Kettunen, "An enhanced multi-position calibration method for consumer-grade inertial measurement units applied and tested," Meas. Sci. Technol., vol. 21, no. 10, 2010.

[11] B. Xu, L. Wang, and T. Duan, "A novel hybrid calibration method for FOG-based IMU," Measurement, vol. 147, 2019.

[12] P. Wang, Y. Gao, M. Wu, F. Zhang, and G. Li, "In-Field Calibration of Triaxial Accelerometer Basedon Beetle Swarm Antenna Search Algorithm," Sensors (Basel), vol. 20, no. 3, Feb. 2020.

[13] Z. Wang, Y. Xie, X. Yu, H. Fan, G. Wei, L. Wang, Z. Fan, G. Wang and H. Luo, "A system-level calibration method including temperature-related error coefficients for a strapdown inertial navigation system," Meas. Sci. Technol. vol. 32, no. 11, pp. 115117-115125, 2021.

[14] T. Song, K. Li, Q. Wu, Q. Li, and Q. Xue, "An improved self-calibration method with consideration of inner lever-arm effects for a dual-axis rotational inertial navigation system," Meas. Sci. Technol., vol. 31, no. 7, 2020.

[15] Y. Lin, L. Miao, Z. Zhou, and C. Xu, "A High-Accuracy Method for Calibration of Nonorthogonal Angles in Dual-Axis Rotational Inertial Navigation System," IEEE Sensors J., vol. 21, no. 15, pp. 16519-16528, 2021.

[16] P. Hu, P. Xu, B. Chen, and Q. Wu, "A Self-Calibration Method for the Installation Errors of Rotation Axes Based on the Asynchronous Rotation of Rotational Inertial Navigation Systems," IEEE Trans. Ind. Electron., vol. 65, no. 4, pp. 3550-3558, 2018.

[17] M. Dai, and J. Lu, "A Full-Parameter Self-Calibration Method Based on Inertial Frame Filtering for Triaxis RINS Under Swaying Base," IEEE Sensors J., vol. 19, no. 6, pp. 2170-2180, 2019.

[18] Y. Liang, L. Han, X. Dong, Q. Li, and Z. Ren, "An quantitative method for observability analysis and its application in SINS calibration," Aerosp. Sci. Technol., vol. 103, pp. 105881-105889, 2020.

[19] S. Wang, G. Yang, and L. Wang, "An Improve Hybrid Calibration Scheme for Strapdown Inertial Navigation System," IEEE Access, vol. 7, pp. 151669-151681, 2019.

[20] J. Li, F. Jiao, J. Fang, and Y. Ma, "Integrated calibration method for dithered RLG POS using a hybrid analytic/Kalman filter approach," IEEE Trans. Instrum. Meas., vol. 62, no. 12, pp. 3333-3342, Dec. 2013.

[21] P. Gao, K. Li, L. Wang, and Z. Liu, "A self-calibration method for tri-axis rotational inertial navigation system," Meas. Sci. Technol., vol. 27, no. 11, 2016.

[22] L. Camberlein and F. Mazzanti, "Calibration technique for laser gyro strapdown inertial navigation systems," Ortung und Navigation, 1985.

[23] Q. Cai, G. Yang, N. Song, and Y. Liu, "Systematic Calibration for Ultra-High Accuracy Inertial Measurement Units," Sensors (Basel), vol. 16, no. 6, Jun 22, 2016.

[24] B. Yuan, D. Liao, and S. Han, "Error compensation of an optical gyro INS by multi-axis rotation," Meas. Sci. Technol., vol. 23, no. 2, 2012.

[25] Y. Mao, J. Dai, Y. Yang, T. Li, and C. Chen, "Star sensor installation error calibration technique with single star simulator and two-position overturning," 7th Annu. Seminar Chin. Acad. Inertial Technol., pp. 104-107, Oct. 2015.

[26] J. Gao, Y. Zhang, J. Gao, K. Zhang, M. Guo, "Star Sensor Calibration Using Fine Guidance Sensor Information for Installation Errors," Journal of Physics Conference Series, vol. 1971, no. 1, pp. 012015-012021, 2021.

[27] Y. Wang, "A high accuracy calibration method of the installation error between SINS and star sensor," Control Technol. Tactical Missile, vol. 26, no. 3, pp. 17-20, Sep. 2009.

[28] Y. Yang, C. Zhang, J. Lu, and H. Zhang, "In-Flight Calibration of Gyros

and Star Sensor With Observability Analysis for SINS/CNS Integration," IEEE Sensors J., vol. 17, no. 21, pp. 7131-7142, 2017.

[29] M. Wu, Y. Wu, X. Hu, and D. Hu, "Self-calibration for land navigation using inertial sensors and odometer: Observability analysis," AIAA Guidance, Navigation and Control Conference, Chicago: pp. 1-10, 2011.

[30] Y. Tang, Y. Wu, M. Wu, and D. Hu, "INS/GPS integration: Global observability analysis," IEEE Trans. Veh. Technol., vol. 58, no. 3, pp. 1129-1141, 2009.

Zhihao Xu was born in 1994. He received the bachelor's degree and the master's degree from the Xi'an high-tech research institute, Xi'an, China. He is currently pursuing the Ph.D. degree with Xi'an high-tech research institute. His research interests are related to inertial navigation and integrated navigation.
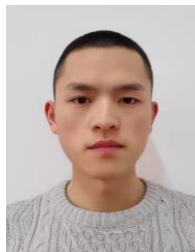
Zhaofa Zhou was born in 1973. He received the Ph.D. degree from the Xi'an high-tech research institute, Xi'an, China. He is currently a Professor with the Xi'an high-tech research institute. His current research interests are integrated navigation and control engineering.
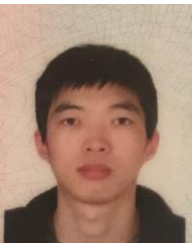
Zhenjun Chang was born in 1986. He received the Ph.D. degree from the Xi'an high-tech research institute, Xi'an, China. He is currently a Lecturer with the Xi'an high-tech research institute. His current research interests are integrated navigation and control engineering.

Shiwen Hao was born in 1996. He received the bachelor's degree from the Beijing University of Science and Technology, Beijing, China. He is currently pursuing the Ph.D. degree with Xi'an high-tech research institute. His research interests include gravity measurement and inertial navigation.

Hui Duan was born in 1996. He received the bachelor's degree from the Wuhan University of Technology, Wuhan, China. He is currently pursuing the Ph.D. degree with Xi'an high-tech research institute. His research interests include celestial navigation and machine learning.